Materials and Design 157 (2018) 227–234

Contents lists available at ScienceDirect

Materials and Design

journal homepage: www.elsevier.com/locate/matdes

In-process measurement and monitoring of a polymer laser sintering powder bed with fringe projection

Nicholas Southon [a,b,*], Petros Stavroulakis [a], Ruth Goodridge [b], Richard Leach [a]

[a] Manufacturing Metrology Team, Faculty of Engineering, University of Nottingham, UK
[b] Centre for Additive Manufacturing, Faculty of Engineering, University of Nottingham, UK

HIGHLIGHTS

- In-process fringe projection measurements provide early detection of defects.
- Height drop due to consolidation is a suitable measure of successful processing.
- Maximum height from powder bed surface identifies both random defects and curling.
- The data analysis presented is suitable for process control decisions.

GRAPHICAL ABSTRACT

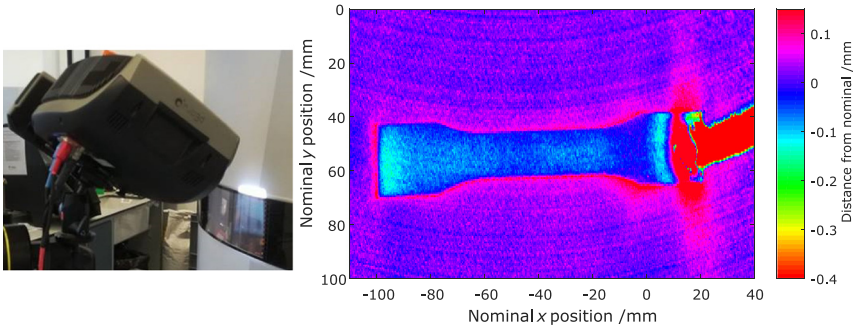

ARTICLE INFO

Article history:
Received 11 May 2018
Received in revised form 23 July 2018
Accepted 24 July 2018
Available online 25 July 2018

Keywords:
Polymer
Laser sintering
Fringe projection
Defect
In-process monitoring
Process signatures

ABSTRACT

We investigate the feasibility of using fringe projection to monitor the powder bed of a polyamide 12 polymer laser sintering machine. In particular, we demonstrate the ability of fringe projection to identify a number of defects arising during the printing process by recording the three-dimensional structure of the sintered powder bed after the completion of each layer. The defects identified ranged in size from hundreds of micrometres to hundreds of millimetres. The three-dimensional analysis of the powder bed data has shown the ability to quantify effects, such as curling, powder spreader blade interactions and the consolidation of a sintered layer. It has, therefore, been shown that the use of fringe projection in polymer laser sintering machines can provide deeper understanding and monitoring of the dynamic behaviour during the process. Fringe projection has shown potential to become part of a feedback and control system that interrupts the build and corrects for in-process defects where possible.

1. Introduction

Additive manufacturing (AM) is a fast growing family of processes that build parts directly from three-dimensional (3D) model data in a layer-by-layer process [1, 2] in contrast to more traditional techniques, such as machining of bulk material, casting and forging. In comparison to classical 'subtractive' production methods, AM is generally characterised as having greater design freedom and reducing material waste [3, 4].

The specific AM process investigated in this work is polymer laser sintering and is part of a family of methods called powder bed fusion (PBF). Despite laser sintering being an established industrial process, the process control available is minimal and generally not closed-loop [4–6]. The subsequent lack of process reliability at the level required by many industries is one of the main reasons why laser sintering is not more widely used for end-use manufacturing [7].

* Corresponding author at: Manufacturing Metrology Team, Faculty of Engineering, University of Nottingham, UK.
E-mail address: Nicholas.Southon@nottingham.ac.uk (N. Southon).

https://doi.org/10.1016/j.matdes.2018.07.053

2. Background

Laser sintering of polymers involves the scanning of a focussed laser spot across a powder bed consisting of polymer particles, usually of around 50 μm in diameter [8]. The powder bed is usually heated to the melting onset point of the material in order to reduce thermal stresses from non-isotropic cooling induced by the laser that could cause the build to fail [8]. When the powder bed is heated to the melting onset point, the scanning laser spot provides enough energy to cause the material under the laser spot to melt without causing significant material degradation [9]. Between layers, the powder bed is lowered by a pre-set layer height, generally double the diameter of the average particle size. Finally, a new layer of powder is prepared for the next laser beam pass, by spreading a thin powder layer across the powder bed. There are many process parameters which contribute to a successful build [10], and both process monitoring and process control are vital to ensuring manufactured parts are within acceptable tolerances.

To identify whether fringe projection can be used to detect and provide feedback on structural defects created during laser sintering of polymers, the parameter ranges where defects are created need to be ascertained. To obtain the appropriate parameter ranges, a mapping of the parameter space is essential to allow monitoring in known processing conditions. This mapping identifies what is measured in both successful and failing builds.

2.1. Process mapping

Process mapping is used to explore the parameter space available in a process, by characterising the outcome of the build with regards to a measured property of the produced part for specific combinations of input parameters. Examples of these properties are surface texture and part porosity [11, 12]. Process mapping enables the determination of the acceptable ranges of important process parameters, which guarantee manufactured part specification within tolerances [13–15]. Of the numerous formalised methods of process mapping, design of experiments [16] and Taguchi [15] are notable examples. Successful mapping allows the selection of specific combinations of parameters which achieve the desired part properties (such as mechanical performance or production time).

Process mapping of AM materials has been carried out previously in a range of laser sintering machines [17–20] and has been used for improving the process parameters for specific structures [15, 21]. However, these improved parameters are only applicable to the specific combination of machine and material and are only found after numerous test builds have been completed. In this work, we performed an iterative search methodology for process mapping to ensure maximum coverage of failure modes in an EOS P100 laser sintering machine with 50% recycled polyamide 12.

2.2. Process monitoring

To ensure the builds remain within the desired parameter ranges, process monitoring and control are required, even with a complete process map. Process monitoring and control are especially required where the acceptable parameter ranges are small or when the parameters are pushed to the limits of their ranges for a specific reason (e.g. maximum scan speed), and temporal variation is critical. Process control takes in-process measurements of process signatures as input [22]. Examples of laser sintering process signatures include height drop due to consolidation, curling of consolidated parts and the temperature of the polymer illuminated by the laser spot. Measurements of process signatures enable closed-loop control of process parameters to keep the produced part within specified tolerances, something which is in high demand from industry [4]. An implemented alternative to process control, used to counteract the uncertainties of end part geometries and properties, is computer simulations [23, 24]. Whilst simulation can help to reduce the occurrences of reproducible errors or distortions, it does not improve control over errors caused by the inherent variability in the AM process.

Process monitoring has already been developed for metal PBF. These systems of process monitoring and control can be applied to polymer laser sintering and so these techniques will be referenced in this document. Comparisons can be made between techniques which view the whole bed at once [25, 26], with those that scan the powder bed [27] often in tandem with the laser spot [28–30]. Literature on techniques that view the whole bed at once mainly focus on measuring the geometry of the consolidated material, generally relying on high resolution imaging [31–33]. Current methods of measuring such defects, including differential lighting [31, 32], do not give a measurement of the height above the powder bed, and they do not give conclusive information about the process instability measured. Fringe projection provides quantitative height information and insight into process stability, enabling deeper understanding of the production of parts.

2.3. Fringe projection

The monitoring technique used in this work to identify structural defects was fringe projection [34, 35]. Fringe projection was selected as it is more suitable to be used in-process because of the ability for real-time data processing [36–38]. Furthermore, fringe projection has been shown to operate well with diffusely scattering white materials such as polyamide 12 [39, 40].

In fringe projection, a camera observes the distortions of a light pattern projected onto the object's surface induced by the object's shape, see Fig. 1. Several depth cues can be used in the reconstruction of the surface shape and the least-squares phase shifting algorithm was used for reconstruction in this study [41]. This specific algorithm uses N images of projected sinusoidal fringe patterns that are phase shifted by $2\pi/N$ with respect to the previous pattern.

The irradiance distribution of the fringe patterns is given by

$$I_i(x,y) = I_0\left[1 + \cos\left(\frac{2\pi x}{p} + \delta_i\right)\right] \quad (1)$$

where i denotes the i^{th} image, I_0 is the modulation of the irradiance, p is the sine wave period and δ_i is the absolute phase for the i^{th} image. In most implementations, $N \geq 3$ since there are three unknowns when solving for the surface height. The N measurements of the fringe

Fig. 1. A sinusoidal fringe pattern projected onto a polymer AM part from the bottom right hand corner of the image. The irradiance distribution across the part is used to reconstruct the surface.

illuminated surface can be combined to form a wrapped phase map, given by

$$\phi(x,y) = \arctan\left(\frac{-\sum_{i=1}^{N} \sin(\delta_i) I_i(x,y)}{\sum_{i=1}^{N} \cos(\delta_i) I_i(x,y)}\right) \quad (2)$$

where $\phi(x,y)$ takes wrapped values of $[-\pi,\pi]$ because of the properties of the arctangent function. Retrieving the non-wrapped phase values (phase unwrapping) and can be achieved either with more information (generally additional measurements of different patterns) or with local searches for phase jumps indicating where the data is wrapped. It is possible to use more than one fringe projection technique to recover surface heights, combining high quality wrapped phase data with lower resolution data with little or no phase ambiguity. Some popular hybrid analysis techniques are covered in [36]. The unwrapping used here combines phase stepped sinusoidal fringe patterns with binary patterns to unambiguously unwrap phase data.

Fringe projection has been suggested for post-process optical form metrology of metal AM parts [34], as well as being demonstrated in metal PBF as an in-situ powder bed measurement technique [42]. Whilst it has been demonstrated in polymer PBF [40], the current literature does not demonstrate process control signals other than geometric contour deviations of consolidated areas. This paper presents process signatures of laser sintering measured with fringe projection across a large portion of the powder bed of an EOS P100 laser sintering system. The measured process signatures allow the quality and stability of the processing to be determined and the process signatures would likely apply across most powder bed fusion processes. The potential for incorporating fringe projection measurements into a closed-loop process control system is also discussed.

3. Experimental work

Process mapping of the laser sintering system was completed before process monitoring with fringe projection. This was done to place the process monitoring measurements within the context of the process map, to confirm the observed processing regimes. All builds were carried out with an EOS P100 laser sintering machine using 50% recycled polyamide 12 from EOS, PA2200, with an average particle size of 56 μm and specified built tensile strength of 48 MPa. Some builds, chosen due to their position in the process map, were measured in-process with a commercial fringe projection system (NUB3D SIDIO XR).

3.1. Process mapping

As explained in Section 2, process mapping was carried out to link the structural defects measured in-process via fringe projection whilst varying scan speed, laser power and build temperature. For the parameters which were not varied during the experiments (layer height, hatch spacing, hatch offset, etc.), settings derived from previous experience with the polyamide 12 material on the specific machine were used.

3.1.1. Build temperature

Parts were produced at various nominal powder bed surface temperatures, ranging from 150 °C to 174 °C. Many builds at 174 °C completed successfully, although some parts were very fragile, showing the wide range of process parameters with which polyamide 12 can be used. The only failure mode observed in the high-temperature processing was polymer degradation, which can cause polymer particulates to obscure the laser glass and cause a degradation of mechanical properties. At the lowest temperatures, successful sintering was not achieved because, when enough energy was delivered to consolidate the powder, curling caused build failure. A potential cause of this failure mode is excessive thermal differentials and rapid cooling due to a cold powder bed. As can be seen in Fig. 2, the lower the temperature of the build, the earlier failure by blade interaction tended to occur. Failures consisted of at least one sample being dragged across the powder bed by the recoater blade or no sintering being visible through the observation window. Fig. 2 also allows spatial grouping and delineation of process modes and the parameters that are required to produce them. The set of parameters associated with lack of sintering and polymer degradation is dependent on the temperature of the powder being sintered. This temperature dependence is because less energy is required to cause polymer degradation when the starting temperature is higher. The opposite applies to lack of sintering. Whilst most discussions of energy density in laser sintering do not consider this role of powder bed temperature, these results illustrate the importance of its consideration.

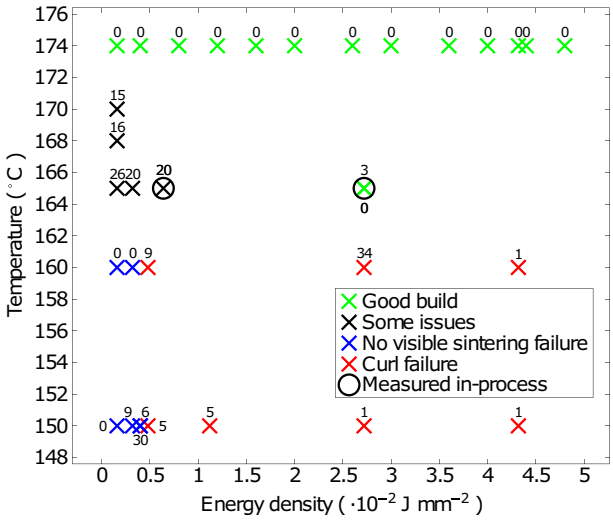

Fig. 2. A process map detailing how the failure modes change with both energy density and powder bed temperature. The layers on which failures or blade interactions occurred are denoted by the numerical labels on points. Greater detail of the two builds measured in-process are detailed in the Results section.

3.1.2. Laser power and scan speed

An iterative search methodology was chosen for the process mapping of the scan speed and laser power in the P100 to identify regions of failure in the process map. This ensured coverage of failure modes without wasting too many builds on parameter combinations that would fail to print. The hatch spacing was fixed at 250 μm, a common beam overlap ratio. The process mapping also does not consider the possibilities of using multiple laser scan passes per layer, which delivers the laser heating in several passes, thus reducing the stresses in the coalesced regions [43]. The application of this scan strategy should make higher energy density parameter combinations possible at the expense of the time taken to repeat scanning of layers multiple times. Another consideration is that the rate of cooling experienced by a polymer part produced with laser sintering influences the crystallisation process, which in turn, influences the mechanical properties of the part [44]. It should be noted that, because parts were built at different heights in the build volume, it is possible that the cooling rates of parts varied throughout [45].

3.2. Fringe projection measurements

In-process fringe projection measurements of the laser sintering powder bed surface were made with a NUB3D SIDIO XR. The nominal measurement pitch was 75 μm in all three orthogonal directions, with a scanning volume of 200 mm × 150 mm × 90 mm, and a stated volumetric accuracy after calibration of 15 μm. The powder bed was viewed through the operator observation window of the machine. On the P100, this consists of an outer curved acrylic window and a thermally insulated flat glass window. For the in-process measurements of the powder

bed surface, the viewing angle was roughly 55° from horizontal. The builds consisted of single tensile test specimens, with best measurement results when the test specimens were closer to the front of the build chamber, due to reduced data drop out. The measurements were manually timed for when the sintering of the closest tensile test piece to the window had finished. When the laser scan path was not visible, due to insufficient sintering, manual timing was employed to ensure the measurement was started at the correct point in the overall laser scan path progression. When the measurements were made at incorrect times, this was noted and quantified. The issues that arose were early or late triggering of the scan, with some late triggering of the scan leading to the powder recoater blade entering the scanning volume or the powder bed being lowered for the next layer. The scans consisted of camera exposure times of 300 ms, 400 ms and 500 ms, which were each completed with a series of projected binary fringes followed by a series of phase shifted sinusoidal patterns being projected. This hybrid approach allows for the low phase ambiguity of binary fringes to augment the greater height sensitivity of sinusoidal fringe projection. The commercial control software then created a wrapped phase map from the fringe images before creating an unwrapped phase map. The unwrapped phase map could then be converted into a point cloud with real-world co-ordinates because of calibration prior to the measurements [46, 47]. This calibration consisted of moving a checkerboard target with calibrated intersections of squares along the optical axis of the instrument at known intervals using a motorised lead screw.

4. Results

Each point cloud measurement acquired consisted of approximately 290,000 points, with a lower density of points in the negative nominal *y* direction. To remove constant planar distortions present in the measurements, the point clouds were subtracted from the reference point cloud scan of a nominally flat powder bed surface. The difference of two powder scans on consecutive layers shows 95% of the data is ±65 μm with a mean of 6 μm and there is no systematic form error. The mean difference between the powder scans is within the stated accuracy of the SIDIO XR. The magnitude of uncertainty within these results is small compared to the process signatures considered, hence a flat clear powder surface is an adequate reference from which to perform our measurements. The categories of structural defects relevant to process control, identified using the fringe projection system and data analysis are presented below.

4.1. Curl

Fig. 3 shows a height map of the final sintered layer of a part with severe curling. Not only are the sintered areas above the powder bed surface, heaping of surrounding powder can also be seen, especially around −30 mm in the *x* direction. The slope of the heaped powder extends at least 10 mm from the consolidated part.

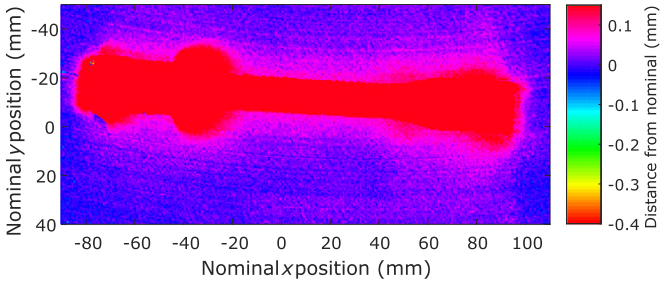

Fig. 3. Height map of the 30th and final layer of a successful build with significant curling, processed at 165 °C, 4 W with a scan speed of 2500 mm/s. The maximum curl at both edges is over 1 mm, which includes the contribution of rocking caused by the part interacting with the blade. Fig. 5 shows this effect across the many layers of the build. The height of most of the part is measured as >0.1 mm so it has one uniform colour.

Fig. 4 demonstrates that, even in a build which did not end in catastrophic blade interactions, the part's effect on the powder was still visible after 2.9 mm of powder had been spread on top of the completed part. The features are about 50 μm from nominal, close to the average particle size. It can be seen that curling failure is easy to detect and analyse, which is covered in greater detail in 0.

4.2. Powder bed surface irregularities

Fig. 4 shows smaller powder bed surface irregularities, which were seen on every layer, as well as the larger-scale lifting of the powder bed caused by underlying sintered regions deforming. Because the small-scale irregularities were arc shaped, they were attributed to spreader blade issues. The issues likely arose from particles attached to the powder spreader blade, leaving grooves roughly one particle diameter deep. Both categories of defects are desirable to detect, and the fringe projection measurements are suitable for both. It is not clear why the curled ends of the part cause a raised area on the left hand side and a depressed area on the right hand side.

4.3. Blade interactions

The rocking motion shown in Fig. 5 is caused by the powder spreader blade catching the trailing end of the part and pushing it deeper into the powder bed. This severity of interaction between blade and part often leads to a part being dragged out of the powder bed and a failed build, but in this instance, the build completed. The onset of the blade interactions appears to occur when the maximum height of the part is approximately 500 μm above nominal powder bed height. The increased rate of warping after the part starts interacting with the blade can be seen in Fig. 8.

4.4. Level drop due to consolidation

The reduction in height of a layer due to consolidation, through melting of the polymer powder bed is a direct measure of successful densification in laser sintering of a polymer [48], visible in Fig. 6. A clearer visualisation of the trend of height drop due to consolidation can be seen in Fig. 7. Defect detection is also demonstrated in the sintered area of layer 16. The inset shows the broken end of the specimen which had been caught by the powder recoating blade. The remaining defect in the sintered region reduces in size in subsequent layers and is hard to discern by layer 22.

4.5. Process control signals

Reducing the point cloud data of the powder bed surfaces to numerical quantities representative of performance allows for simple process control decisions. Two such measures are presented here.

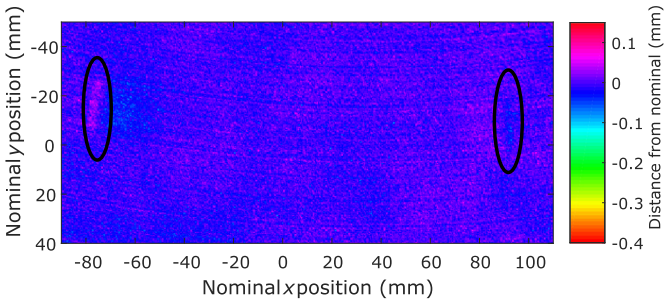

Fig. 4. Height map showing twenty-nine layers of fresh powder after the final sintered layer seen in Fig. 3. The continuing effect of the curled ends of the part can be seen. The ovals indicate the positions of both ends of the part.

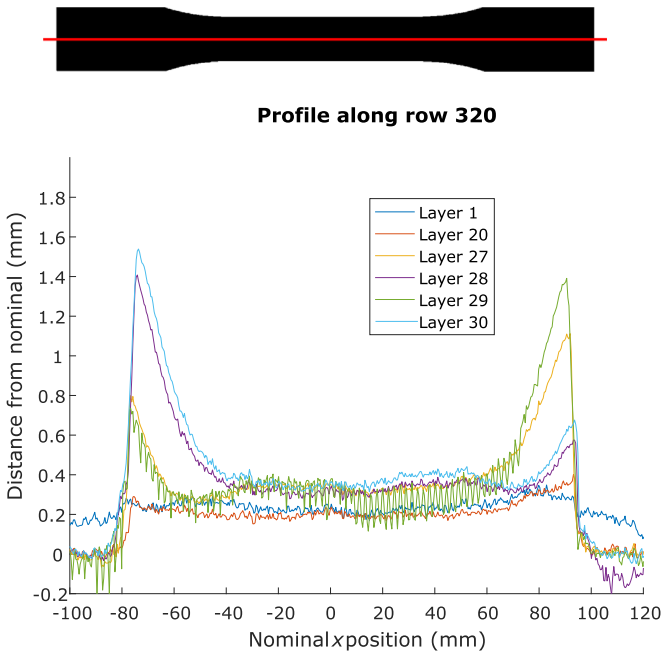

Fig. 5. A profile along the centre of the tensile test specimen, as shown above, processed at 165 °C, 4 W and a scan speed of 2500 mm/s. High spatial frequency artefacts in the data for some layers are due to the bed being lowered before all the fringe projections had been completed. Towards the end of the build, alternate layers have opposite ends raised.

Fig. 7 shows that height drop due to consolidation is a strong indicator of the success of sintering. It is clear in the first layers of the build whether the parameters are not leading to significant levels of sintering. The increasing height drop due to consolidation as the build progresses is consistent with the geometric series discussed elsewhere [42]. The corresponding graph for the 4 W build shows no discernible trends due to excessive curl and limited consolidation. As the maximum height drop is dependent on both the powder packing efficiency and the degree of consolidation, it is possible to estimate the degree of consolidation in process.

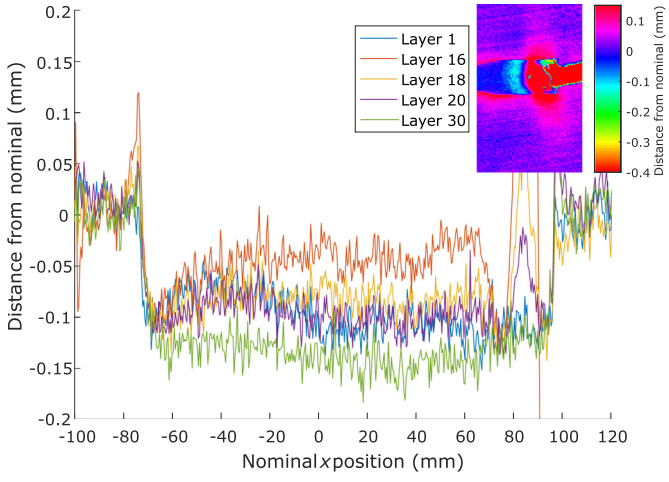

Fig. 6. Tensile test specimen at 165 °C, processed at 17 W with a scan speed of 2500 mm/s. A 100 μm to 150 μm drop due to sintering is observed. Possible causes of the high edges are non-optimised settings for contours, an optical effect of the side of the drop or localised warping at the edge of the part [49, 50]. The profile was taken from the same region as shown in Fig. 5. The inset shows the powder bed after the sintering of layer 16, the part-blade interaction happened when the fresh powder was spread for the sintering of layer 16.

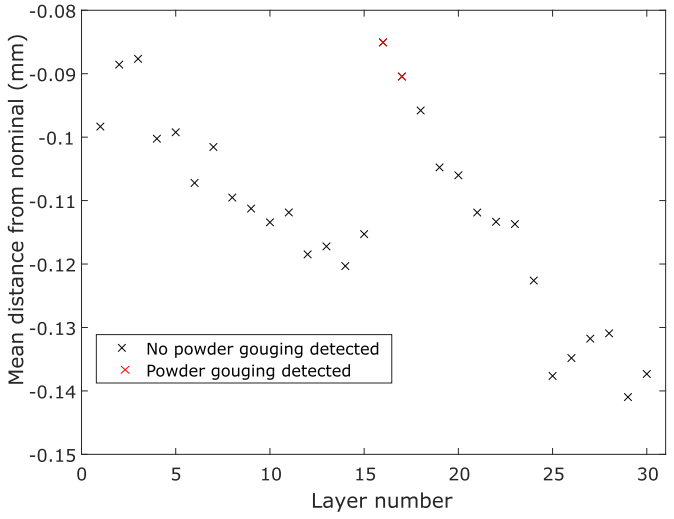

Fig. 7. Mean distance from nominal of consolidated powder for the 17 W build. Powder gouging (indicated with red crosses) was detected when >0.1% of the powder bed was measured at >500 μm below nominal. (For interpretation of the references to colour in this figure legend, the reader is referred to the web version of this article.)

In contrast to height drop due to consolidation, the maximum height of the consolidated area indicates whether sintering is proceeding without curling.

Fig. 8a) shows the effect of an isolated error on the maximum height reached above the powder bed for the 4 W build. Both before and after layer 16, the maximum distance from nominal is about 150 μm. The magnitude of the change makes this derived process signature suitable for in-process control decisions. Fig. 8b) shows the instability of the 4 W parameter choice as the maximum height from the powder bed increases up to the final layer (30) and then decreases as new powder covers the warped part. The inflection point around layer 20 is thought to be because of blade interactions, and is another clear indication of process issues beyond the increasing amount of curling seen before layer 20. It is interesting to note that the maximum height from nominal after layer 30 decreases faster than the lowering of the part due to new layers of powder being spread. This could be the result of the thermal stresses of the part reducing as the rate of heat loss from the top surface is reduced due to the insulating layers of powder spread on top.

5. Discussion

It has been shown that the fringe projection measurements of the powder bed were successful in detecting several process signatures. The analysis of these signatures, shown in Figs. 7 and 8 enabled the prediction of the final outcomes of the builds.

As can be seen in Fig. 2, the transition from no visible consolidation to a build failure due to curling occurs at far lower energy densities than the builds with the most successful layers. Therefore, having just enough energy to consolidate the layer is not the optimal processing point at the specified temperature, due to the severe curling. The general trend discovered was that as the temperature was increased the parts built for more layers before an error occurred. The inconsistency of results found may be due to variability in the process. Under high-temperature conditions, it was noted that a complete lack of sintering was not observed in any builds. However, the parts created with the lowest energy density were considerably weaker than other test specimens, causing one of the three samples to break as it was removed from the build chamber. In the low-temperature conditions, the parameter sets that led to no sintering showed no visible indication of sintering during the process. Curling occurred in some builds where no sintering was visible, demonstrating that the naked eye is not always sufficient to identify whether partial consolidation has occurred in areas scanned by

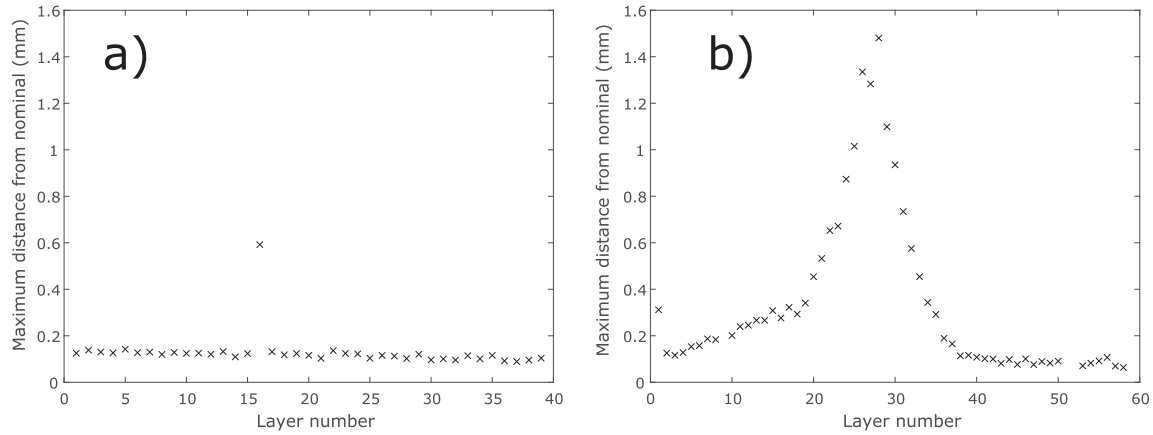

Fig. 8. The evolution of maximum height of the consolidated area for both builds. The influence of erroneously measured points was mitigated by removing the top 0.01% of data which has not changed the overall trend of results. a) 17 W build with the defect in layer 16 shown by the outlying point b) 4 W build with a clear deviation from the steady state results shown in a).

the laser. These results show the need for high-quality process monitoring for automated classification of the process outcomes.

It should be noted that smaller particles are preferentially heated when the laser imparts energy [51], due to the volume of polymer requiring heating being smaller. This preferential heating causes higher peak temperatures and greater chances of polymer degradation. Therefore, particle size distribution needs consideration when process monitoring and control are performed. Also, since all values for laser power and scan speed are nominal, it is conceivable that the recorded values of both deviate significantly from the actual values.

There were no occurrences of catastrophic curling at the highest temperature builds because excessive polymer degradation (i.e. producing thick white smoke) occurs at a lower energy density than the point where induced residual stresses cause failure of the build. Even when parts were successfully built at lower temperatures, blade interactions occurred. For the build shown in Fig. 5, the highest point of the consolidated area alternates between the left and right hand sides towards the end of the build, when the magnitude of the curl is greatest. This pattern of data can be interpreted as the part being rocked by the blade as it spreads a new layer of powder, tipping up the end of the part over which the blade passed first. The overall shape of the lengthwise cross sections agrees with previous literature that describes the large radius of the main curve of the part, along with increased curling at the extreme edges of a part [49, 50]. Three phenomena have been linked to curling: thermal differentials causing differential stresses, densification and shrinkage upon cooling [4, 49]. It has also been shown that the cooling rate of polymer laser sintered parts has a measurable impact on mechanical properties [52]. In contrast to the curling, which gets worse with each new layer, Fig. 6 shows evidence of self-repair of a potentially catastrophic defect. This self-repair shows how the evolution of a defect needs to be understood before process control remedies can be considered. It also demonstrates how large defects could be hidden inside AM parts with little to no external indication of issues. The detection of both these failure modes is important because quickly detecting when a build is likely to fail could save significant time and cost when producing small numbers of AM parts.

Energy density, also known as the Andrew number, is a commonly used measure of delivered energy in laser sintering [53, 54]. Despite being a common metric to compare different process parameter combinations, there are various issues with energy density as a normalising value. Firstly, the areal energy density is generally used since layer height is commonly kept constant in experiments, but varying layer height will invalidate comparisons based on areal energy density. Dividing the areal energy density by the layer height gives the volume energy density, the measure of delivered laser irradiation per unit volume. Using the volume energy density corrects for layer height variation, but it still does not address fundamental issues with the complexities of the process that are ignored when only the laser energy input is considered. Energy density proves a popular normalising value because collapsing two-dimensional parameter variations into a single value creates clearer graphs, see Fig. 2. However, two sets of process parameters with equal energy density can lead to two different processing outcomes, as shown in the insets. As well as this, different materials cannot be simply compared due to the variations in required energy delivery to melt the powder bed. The inability to simply compare across materials reduces the utility of previous material studies for new materials. It is also worth noting that processing with multiple laser passes cannot be captured simply with energy density because heat loss is not taken into account. This shows that energy density is an incomplete reduction of the energy delivery process into a single value [53]. Hann et al. [55] proposed normalising with respect to enthalpy and melt pool depth for laser welding. The utility of their approach has been validated for experimental and simulated laser melting data [56]. However, if parameters other than scan speed, laser power and hatch spacing are kept constant, energy density can be useful as a normalised value with which to compare properties across various builds. These comparisons allow a wide range of process parameters to be considered when optimising builds.

Of the many potential failure modes in laser sintering [4, 5], the ones observed in these experiments were polymer degradation, lack of sintering, catastrophic curling and excess thickness/width. These results suggest numerous avenues for future work. Repeating similar experiments on differing machines with different measurement strategies would investigate the universality and detectability of the process signatures discussed here. How surface topography evolves when defects occur is another important question. If process monitoring detects a defect in the powder bed surface, only detailed knowledge of the expected evolution of such a surface can determine whether process control needs to intervene. This detailed knowledge can be obtained through three-dimensional measurements of the powder bed surface during the process. More detailed analysis of the built parts would help to create a clearer picture of the mechanisms by which process signatures impact final part properties. For example, the drop due to consolidation could act as an indication of consolidation success. Improved frameworks for the analysis of the in-process surface measurements are also required. One example is determining the best solutions for efficient CAD comparison and process success categorisations; without these frameworks process control cannot be reliably implemented.

6. Conclusions

In summary, this work shows that fringe projection can be used for in-process monitoring of polymer powder bed fusion to prevent structural defects forming during the build. Fringe projection can quickly

detect structural defects which are potentially catastrophic to the build such as curling and irregular level drops, and is, therefore, suitable for dynamic process control. The information gained during the process could be used to perform in-situ modifications of process parameters as well as to repair detected defects [57].

Curling, which is always undesirable and can be used as a signal that intervention is required from process control, was one of the strongest in-process signatures measured. However, the link between curling and final part properties cannot be easily drawn since polymer degradation occurs before curling at optimal temperatures.

The presented measurements also place bounds on the sensitivity of both direct and indirect depth measurements required for in-process monitoring of the laser sintering powder bed. The process signatures discussed are likely to be universal across all powder bed fusion techniques, though the measurement methods required might vary across specific processes.

Fringe projection has been demonstrated in detecting both quality of consolidation and magnitude of curl through analysis of the powder bed surface topography, suggesting this technique could be incorporated into a process monitoring system for laser sintering. The commercial measurement system gave acceptable data quality for a significant area of the build, but a fully integrated system could improve on speed of acquisition and resolution.

Author contributions

Nicholas Southon: Conceptualization, Methodology, Software, Investigation, Writing-Original Draft, Writing-Review & Editing, Visualisation,

Petros Stavroulakis: Resources, Writing-Review & Editing.

Ruth Goodridge: Supervision, Writing-Review & Editing.

Richard Leach: Supervision, Writing-Review & Editing.

Acknowledgements

This work was supported by the Engineering and Physical Sciences Research Council [grant number EP/M008983/1, EP/L01534X/1] and by the BMW Group.

Data availability

The raw and processed data required to reproduce these findings is available on request.

Appendix A. Supplementary data

Supplementary data to this article can be found online at https://doi.org/10.1016/j.matdes.2018.07.053.

References

[1] Anon, Standard Terminology for Additive Manufacturing – General Principles – Terminology, ASTM International, 2015.
[2] I. Gibson, D.W. Rosen, B. Stucker, Additive Manufacturing Technologies: 3D Printing, Rapid Prototyping and Direct Digital Manufacturing, Springer, New York; London, 2015.
[3] K. Kellens, E. Yasa, Renaldi, W. Dewulf, J.P. Kruth, J.R. Duflou, Energy and resource efficiency of SLS/SLM processes, Proceedings of the Solid Freeform Fabrication Symposium Solid Freeform Fabrication Symposium (Austin, TX), 2011.
[4] M. Grasso, B.M. Colosimo, Process defects and in situ monitoring methods in metal powder bed fusion: a review, Meas. Sci. Technol. 28 (2017), 044005. .
[5] S.K. Everton, M. Hirsch, P. Stravroulakis, R.K. Leach, A.T. Clare, Review of in-situ process monitoring and in-situ metrology for metal additive manufacturing, Mater. Des. 95 (2016) 431–445.
[6] M. Abdelrahman, T.L. Starr, Feedforward control for polymer laser sintering process using part geometry, Proceedings of the Solid Freeform Fabrication Symposium (Austin, TX), 2015.
[7] D.L. Bourell, T.J. Watt, D.K. Leigh, B. Fulcher, Performance limitations in polymer laser sintering, Phys. Procedia 56 (2014) 147–156.
[8] R.D. Goodridge, C.J. Tuck, R.J.M. Hague, Laser sintering of polyamides and other polymers, Prog. Mater. Sci. 57 (2012) 229–267.
[9] A. Wegner, G. Witt, S.C. Jana, Understanding the decisive thermal processes in laser sintering of polyamide, AIP Conference Proceedings, 12, 2015, p. 1664 , (160004).
[10] T.G. Spears, S.A. Gold, In-process sensing in selective laser melting (SLM) additive manufacturing, Integr. Mater. Manuf. Innov. 5 (2016) 1–25.
[11] G. de Oliveira Setti, M. Fernandes de Oliveira, I. Alves Maia, J. Vicente Lopes da Silva, R. Savu, E. Joanni, Correlation between mechanical and surface properties of SLS parts, Rapid Prototyp. J. 20 (2014) 285–290.
[12] M. Pavan, T. Craeghs, P.V. Puyvelde, J. Kruth, W. Dewulf, Understanding the link between process parameters, microstructure and mechanical properties of laser sintered PA12 parts through X-Ray Computed Tomography, Proc. of the 2nd Intl. Conf. on Progress in Additive ManufacturingResearch Publishing, 2016.
[13] T. Scharowsky, A. Bauereiß, C. Körner, Influence of the hatching strategy on consolidation during selective electron beam melting of Ti-6Al-4V, Int. J. Adv. Manuf. Technol. 1–10 (2017).
[14] N. Kumar, H. Kumar, J.S. Khurmi, Experimental investigation of process parameters for rapid prototyping technique (selective laser sintering) to enhance the part quality of prototype by taguchi method, Procedia Technol. 23 (2016) 352–360.
[15] N. Raghunath, P.M. Pandey, Improving accuracy through shrinkage modelling by using Taguchi method in selective laser sintering, Int. J. Mach. Tools Manuf. 47 (2007) 985–995.
[16] F. Pukelsheim, Optimal Design of Experiments (SIAM), 1993.
[17] H.C.H. Ho, I. Gibson, W.L. Cheung, Effects of energy density on morphology and properties of selective laser sintered polycarbonate, J. Mater. Process. Technol. 89–90 (1999) 204–210.
[18] T.L. Starr, T.J. Gornet, J.S. Usher, The effect of process conditions on mechanical properties of laser-sintered nylon, Rapid Prototyp. J. 17 (2011) 418–423.
[19] M. Vasquez, B. Haworth, N. Hopkinson, Methods for quantifying the stable sintering region in laser sintered polyamide-12, Polym. Eng. Sci. 53 (2013) 1230–1240.
[20] B. Caulfield, P.E. McHugh, S. Lohfeld, Dependence of mechanical properties of polyamide components on build parameters in the SLS process, J. Mater. Process. Technol. 182 (2007) 477–488.
[21] B. Partee, S.J. Hollister, S. Das, Selective laser sintering process optimization for layered manufacturing of capa® 6501 polycaprolactone bone tissue engineering scaffolds, J. Manuf. Sci. Eng. 128 (2005) 531–540.
[22] M. Mani, B.M. Lane, M.A. Donmez, S.C. Feng, S.P. Moylan, A review on measurement science needs for real-time control of additive manufacturing metal powder bed fusion processes, Int. J. Prod. Res. 55 (2017) 1400–1418.
[23] W. King, A.T. Anderson, R.M. Ferencz, N.E. Hodge, C. Kamath, S.A. Khairallah, Overview of modelling and simulation of metal powder bed fusion process at Lawrence Livermore National Laboratory, Mater. Sci. Technol. 31 (2015) 957–968.
[24] X. Zhao, A. Iyer, P. Promoppatum, S.-C. Yao, Numerical modeling of the thermal behavior and residual stress in the direct metal laser sintering process of titanium alloy products, Addit. Manuf. 14 (2017) 126–136.
[25] M. Abdelrahman, T.L. Starr, Quality certification and control of polymer laser sintering: layerwise temperature monitoring using thermal imaging Int, J. Adv. Manuf. Technol. 84 (2015) 831–842.
[26] J. Mireles, S. Ridwan, P.A. Morton, A. Hinojos, R.B. Wicker, Analysis and correction of defects within parts fabricated using powder bed fusion technology, Surf. Topogr. Metrol. Prop. 3 (2015), 034002. .
[27] G. Guan, M. Hirsch, Z.H. Lu, D.T.D. Childs, S.J. Matcher, R. Goodridge, K.M. Groom, A.T. Clare, Evaluation of selective laser sintering processes by optical coherence tomography, Mater. Des. 88 (2015) 837–846.
[28] P. Lott, H. Schleifenbaum, W. Meiners, K. Wissenbach, C. Hinke, J. Bültmann, Design of an optical system for the in situ process monitoring of selective laser melting (slm), Phys. Procedia 12 (Part A) (2011) 683–690.
[29] I. Yadroitsev, P. Krakhmalev, I. Yadroitsava, Selective laser melting of Ti6Al4V alloy for biomedical applications: temperature monitoring and microstructural evolution, J. Alloys Compd. 583 (2014) 404–409.
[30] T. Craeghs, F. Bechmann, S. Berumen, J.-P. Kruth, Feedback control of layerwise laser melting using optical sensors, Phys. Procedia 5 (Part B) (2010) 505–514.
[31] M. Abdelrahman, E.W. Reutzel, A.R. Nassar, T.L. Starr, Flaw detection in powder bed fusion using optical imaging, Addit. Manuf. 15 (2017) 1–11.
[32] B.K. Foster, E.W. Reutzel, A.R. Nassar, B.T. Hall, S.W. Brown, C.J. Dickman, Optical, layerwise monitoring of powder bed fusion, Proceedings of the Solid Freeform Fabrication Symposium (Austin, TX), 2015.
[33] J. zur Jacobsmühlen, S. Kleszczynski, G. Witt, D. Merhof, Compound quality assessment in laser beam melting processes using layer imagesIEEE International Instrumentation and Measurement Technology Conference (Turin, Italy), 2017.
[34] P.I. Stavroulakis, R.K. Leach, Invited Review Article: Review of post-process optical form metrology for industrial-grade metal additive manufactured parts, Rev. Sci. Instrum. 87 (2016), 041101. .
[35] S.S. Gorthi, P. Rastogi, Fringe projection techniques: whither we are? Opt. Lasers Eng. 48 (2010) 133–140.
[36] S. Van der Jeught, J.J.J. Dirckx, Real-time structured light profilometry: a review, Opt. Lasers Eng. 87 (2016) 18–31.
[37] N. Karpinsky, S. Zhang, High-resolution, real-time 3D imaging with fringe analysis, J. Real-Time Image Proc. 7 (2010) 55–66.
[38] S. Zhang, Recent progresses on real-time 3D shape measurement using digital fringe projection techniques, Opt. Lasers Eng. 48 (2010) 149–158.
[39] M. Launhardt, A. Wörz, A. Loderer, T. Laumer, D. Drummer, T. Hausotte, M. Schmidt, Detecting surface roughness on SLS parts with various measuring techniques, Polym. Test. 53 (2016) 217–226.

[40] Z. Li, X. Liu, S. Wen, P. He, K. Zhong, Q. Wei, Y. Shi, S. Liu, In Situ 3D Monitoring of Geometric Signatures in the Powder-Bed-Fusion Additive Manufacturing Process via Vision Sensing Methods Sensors, 18, 2018 1180.
[41] K. Creath, in: E. Wolf (Ed.), V Phase-Measurement Interferometry Techniques Progress in Optics, vol 26, Elsevier 1988, pp. 349–393.
[42] B. Zhang, J. Ziegert, F. Farahi, A. Davies, In situ surface topography of laser powder bed fusion using fringe projection, Addit. Manuf. 12 (Part A) (2016) 100–107.
[43] R.D. Goodridge, R.J.M. Hague, C.J. Tuck, An empirical study into laser sintering of ultra-high molecular weight polyethylene (UHMWPE), J. Mater. Process. Technol. 210 (2010) 72–80.
[44] P.K. Venuvinod, W. Ma, Rapid Prototyping - Laser-based and Other Technologies, 1st ed Springer US, New York, 2004.
[45] S. Josupeit, H.-J. Schmid, Three-dimensional in-process temperature measurement of laser-sintered part cakes, Proceedings of the Solid Freeform Fabrication Symposium (Austin, TX) 2014, pp. 49–58.
[46] S. Zhang, P.S. Huang, Novel method for structured light system calibration, Opt. Eng. 45 (2006), 083601. .
[47] B. Li, N. Karpinsky, S. Zhang, Novel calibration method for structured-light system with an out-of-focus projector, Appl. Opt. 53 (2014) 3415–3426 (AO).
[48] M. Berzins, T.H.C. Childs, G.R. Ryder, The Selective Laser Sintering of Polycarbonate CIRP Annals - Manufacturing Technology, 45, 1996 187–190.
[49] M. Berzins, T.H.C. Childs, K.W. Dalgarno, G.R. Ryder, G. Stein, Densification and distortion in selective laser sintering of polycarbonate, Proceedings of the solid freeform fabrication symposium, vol 6, 1995, pp. 196–203.
[50] N.M. Jamal, K.W. Dalgarno, Analysis of the influence of viscoelasticity in curl development in sls, Proceedings of the solid freeform fabrication symposium. Texas: Austin Proceedings of the Solid Freeform Fabrication Symposium (Austin, TX), 2002.
[51] K.P. McAlea, P.F. Forderhase, R.B. Booth, Selective Laser Sintering of Polymer Powder of Controlled Particle Size Distribution US5817206 A, 1998 (Issued October 6, 1998).
[52] H. Zarringhalam, Investigation Into Crystallinity and Degree of Particle Melt in Selective Laser Sintering, (Thesis) Loughborough University, 2007.
[53] D. Miller, C. Deckard, J. Williams, Variable beam size SLS workstation and enhanced SLS model, Rapid Prototyp. J. 3 (1997) 4–11.
[54] J.C. Nelson, N.K. Vail, J.W. Barlow, Laser sintering model for composite materials, Proceedings of the Solid Freeform Fabrication Symposium (Austin, TX), 1993.
[55] D.B. Hann, J. Iammi, J. Folkes, A simple methodology for predicting laser-weld properties from material and laser parameters, J. Phys. D. Appl. Phys. 44 (2011) 445401.
[56] W.E. King, H.D. Barth, V.M. Castillo, G.F. Gallegos, J.W. Gibbs, D.E. Hahn, C. Kamath, A.M. Rubenchik, Observation of keyhole-mode laser melting in laser powder-bed fusion additive manufacturing, J. Mater. Process. Technol. 214 (2014) 2915–2925.
[57] M. Hirsch, P. Dryburgh, S. Catchpole-Smith, R. Patel, L. Parry, S.D. Sharples, I.A. Ashcroft, A.T. Clare, Targeted rework strategies for powder bed additive manufacture, Addit. Manuf. 19 (2018) 127–133.